

GT2011-46653

**ESTIMATING THE PROBABILISTIC SIZE AND SHAPE DISTRIBUTIONS OF 3D
ANOMALIES FROM SECTIONING MEASUREMENTS USING THE
STEREOLOGICAL UNFOLDING APPROACH**

Wuwei Liang

Michael P. Enright

Southwest Research Institute®
San Antonio, TX 78238, USA

ABSTRACT

The accuracy of probabilistic risk assessment of rotor disks is strongly dependent on the accurate description of the size and shape distributions of anomalies in alloys. These size-shape distributions of anomalies are often derived from planar sectioning data measurements using stereological unfolding algorithms. Since it is impossible to accurately predict the shape and orientation parameters of a general ellipsoid based on measurements obtained from two-dimensional sectioning data, the anomaly model should be limited to a spheroid. In this study, an unfolding algorithm was implemented and verified that can be used to estimate the probabilistic dimensions and orientations of 3D spheroids based on 2D section data. It is shown that the accuracy of the predicted spheroid model is dependent on the number of sections and the discretization of the mesh used to characterize the data.

NOMENCLATURE

- $f(r)$ = PDF of the radius of circular profiles
- N_A = Number of section profiles per unit area
- N_V = Number of 3D anomalies per unit volume
- P** = Transformation matrix (anomaly size dependent)
- Q** = Transformation matrix (anomaly shape dependent)
- u = Major caliper parameter of a spheroid
- s = Major caliper parameter of the elliptical profile of a spheroid
- v = Shape parameter of a spheroid
- t = Shape parameter of the elliptical profile of a spheroid
- $F_V(u,v)$ = Bivariate size-shape distribution of a spheroid
- $F_A(s,t)$ = Bivariate size-shape distribution of the elliptical profile of a spheroids

1 INTRODUCTION

The presence of rare metallurgical and manufacturing anomalies in turbine disks can contribute to uncontained aircraft engine failures that can lead to catastrophic disasters such as the crash landing at Sioux City, Iowa, in 1989 [1,2]. As a result, probabilistic methodologies have been developed to address the uncertainties associated with fracture-mechanics-based life prediction of aircraft engine components [3-5]. Comprehensive design systems have been developed for the routine assessment of rotors and disks that may contain inherent material anomalies [6-9]. These methodologies provide the capability to quantify the risk of fracture associated with rare, life-limiting events such as inherent material and manufacturing anomalies that occasionally occur during processing. The use of probabilistic methods for risk assessment is now an established practice in the international gas turbine engine industry. For commercial aircraft engines, regulatory agencies recommend probabilistic approaches as part of the certification process, as summarized in several recent U.S. Federal Aviation Administration (FAA) Advisory Circulars [10-12].

The accuracy of probabilistic risk assessment methodologies is closely dependent on the accurate description of the size and shape distributions of anomalies in alloys. In some alloys, this is the dominant random variables affecting the probabilistic risk of fracture [9, 13-14]. Usually, it is very difficult to directly measure the size and shape distributions of 3D anomalies. Indirect anomaly measurement techniques are available, such as Heavy Liquid Separation (HLS) and metallographic examination.

These methods provide 2D information that must be transformed to predict 3D anomaly dimensions. This is a typical problem in stereology, which is the science of estimating higher dimensional information from lower dimensional samples. Wicksell's corpuscle problem is one of the classic problems in stereology [15-16]. He developed an

algorithm to estimate the size distribution of spheres from the size distribution of circular profiles in planar sections [15]. Wicksell later considered the problem of estimating the size and shape distribution of ellipsoids from data measured on the ellipses on planar sections [16]. Although he was able to set out a general relationship linking the moments of the conventional “diameters” of the ellipsoids and the elliptical profiles, Moran [17] and Cruz-Orive [18-19] proved that the ellipsoid problem is indeterminate. They concluded that the equation for the general stereological problem has unique solutions only for particular families of ellipsoids called spheroids, which are biaxial ellipsoids. The spheroids may have random size and shape, not necessarily independent from each other, but they must all be either prolate or oblate for a given model. For prolate spheroids (elongated “football” shape) the major axis is the rotator axis, whereas the minor axis is the rotator axis for oblate spheroids (flattened “pancake” shape).

In this paper, a stereological unfolding algorithm was implemented and verified that can be used to estimate the probabilistic dimensions and orientations of 3D spheroids based on 2D sectioning measurements. The general stereological equation is presented, and an algorithm is described for solving the equation numerically for both prolate and oblate spheroids. The algorithm is then applied to a numerical example where the accuracy of the algorithm is assessed considering the two primary sources of error (statistical and discretization errors).

2 THE SPHERICAL PARTICLE PROBLEM

A general stereological methodology must account for ellipsoidal anomalies of various sizes, aspect ratios, and orientations. To gain an understanding of the equations, it is useful to first assess the simpler sphere problem, which was first presented by Wicksell [15]. Wicksell’s analytical approach requires differentiation of the intercepted size distribution. However, the distribution of circular profiles obtained from experiments is not an analytically smooth profile. Scheil (1931) first addressed this problem by dividing the data into bins [20]. A number of improved methods were later developed based on this discretization approach and the most popular method is the Schwartz-Saltykov method [20, 21]. In this approach, the sizes of the both the particles and their section profiles are divided into an equal number of bins so that the initial differential problem is reduced to a linear algebra problem. Here we illustrate how the Scheil-Schwartz-Saltykov’s discretization method is derived from the analytical continuous size distributions.

Consider a volume containing uniformly distributed spherical particles with radii ranging from 0 to R . If the spheres are randomly sectioned by a number of parallel planes, the radii of circles in the planar sections will also fall in the range from 0 to R . However, the probability density function (PDF) of the sphere radius is not identical to the PDF of the circle radius. In essence, the stereological unfolding problem is to estimate the sphere radius PDF from the circle radius data observed in the planar sections. This problem is illustrated in four steps:

- (1) random sections of a single sphere;
- (2) random sections of a volume with spheres of the same size;
- (3) random sections of a volume with spheres of two different sizes;
- and (4) random sections of a volume with spheres with radii between 0 and R .

2.1 Random Sections of a Single Sphere

Consider a sphere with radius R is sectioned at a distance x from its center, as shown in Fig. 1. The radius of the circle in the section is given by

$$r = \sqrt{R^2 - x^2}, x \in (0, R) \quad (1)$$

If the sphere is sectioned repetitively at random locations, (i.e., x is uniformly distributed between 0 and R , so that $f(x) = \frac{1}{R}, x \in (0, R)$) then the PDF of the circle radius is given by (Fig. 2)

$$f(r) = \frac{1}{R} \frac{r}{\sqrt{R^2 - r^2}}, r \in (0, R) \quad (2)$$

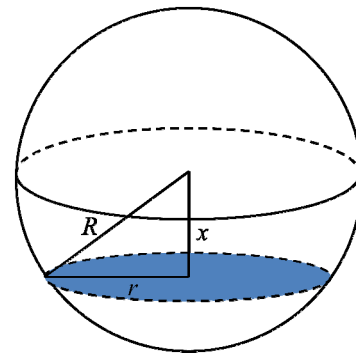


Figure 1. General sphere and associated circular profile at a random planar section.

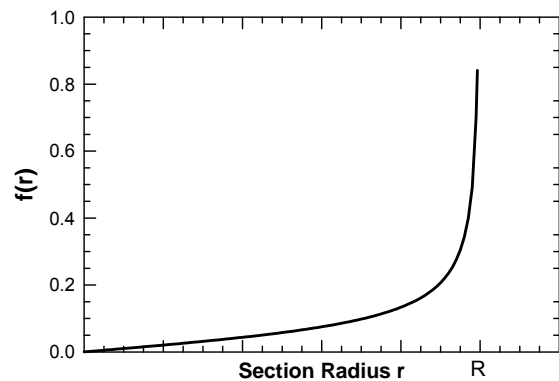


Figure 2. Probability density function of the radii of circular profiles $f(r)$ generated by sectioning a sphere at random locations.

2.2 Random Sections of a Volume with Spheres of the Same Size

If a volume with randomly distributed spheres of the same size is sectioned on random planes, some particles may be sectioned and some may not. The number of spheres that come in contact with a section plane is proportional to the number of spheres per unit volume N_V . Given a unit volume with N_V spheres of radius R per unit volume, the number of circular profiles per unit N_A area is equal to the number of spheres that are sliced by the section plane. As shown in Fig. 3, all spheres with centers falling within thickness of $2R$ will be counted. The number of sliced spheres is given by

$$N_A = 2N_V R \quad (3)$$

Sectioning a volume with randomly distributed spheres of the same size is similar to sectioning a single sphere at random locations. Therefore, the N_A circular profiles have the same size distribution given in Eq. (1). The number of circular profiles with radii between r and $r + dr$ is given by,

$$dN_A = N_A f(r) dr = 2N_V R f(r) dr \quad (4)$$

Therefore, the number of circles within size range (r_1, r_2) is

$$\int_{r_1}^{r_2} dN_A = 2N_V R \int_{r_1}^{r_2} f(r) dr \quad (5)$$

2.3 Random Sections of a Volume with Spheres of Two Sizes

Consider next a volume containing randomly placed spheres of two distinct radii $R/2$ and R with N_{V1} and N_{V2} , spheres per unit volume, respectively. If the spheres of each size are considered separately, the problem can be solved for each sphere using Eq. (2). The distributions for the two sphere sizes ranging from $r \in (0, \frac{R}{2})$ and $r \in (0, R)$ are shown in Figs. 4(a) and (b), respectively. The total size distribution,

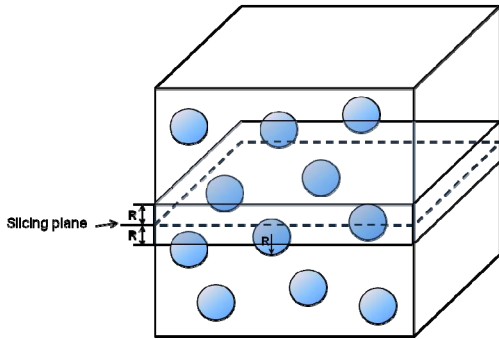
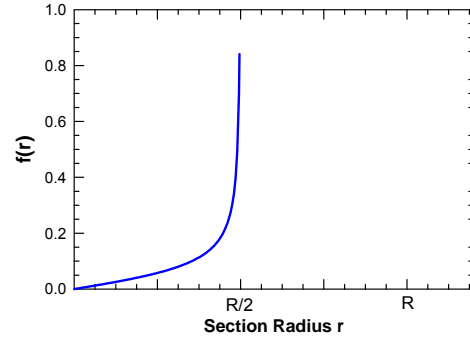
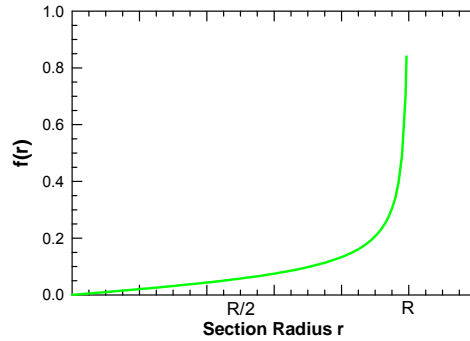


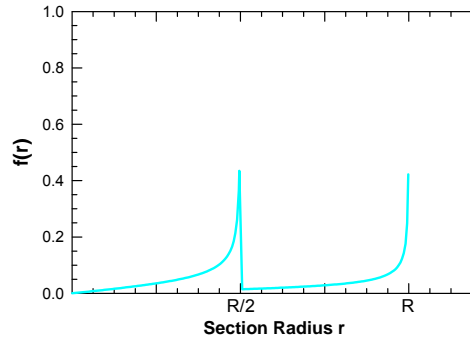
Figure 3. A unit volume with randomly placed spheres intersected by an arbitrary plane.



(a)



(b)



(c)

Figure 4. PDF of the radii of circular profiles associated with spheres of one or two deterministic radii (a) $R/2$, (b) R , and (c) combination of $R/2$ and R .

which consists of circular profiles from spheres of both sizes can be obtained by superimposing the contributions from each size, as shown in Fig. 4(c).

As an illustration, suppose the circle radius values are divided into two bins with size ranges $(0, R/2)$ and $(R/2, R)$. The number of circles in each bin (N_{A1} and N_{A2}) can be derived as follows. The circular profiles of spheres of size $R/2$ all fall with the size range $(0, R/2)$. Substituting sphere radius and size range into Eq. (5) yields,

$$N_{A1,1} = N_{A1} = 2N_V \left(\frac{R}{2}\right) \int_0^{\frac{R}{2}} f(r) dr = N_{V1} R \int_0^{\frac{R}{2}} f(r) dr \quad (6)$$

where $N_{A1,1}$ is the number of circular profiles resulting from spheres of size $R/2$.

The circular profiles of spheres with radius R range between $(0, R)$. Similarly, substituting size ranges of each bin into Eq. (5) yields

$$N_{A1,2} = 2N_{V2}R \int_0^R f(r)dr, \text{ for size bin } (0, R/2) \quad (7)$$

$$N_{A2,2} = 2N_{V2} \int_{R/2}^R f(r)dr, \text{ for size bin } (R/2, R) \quad (8)$$

The total number of circles per unit area in bin $(0, R/2)$, N_{A1} , can be obtained by adding up the contributions from spheres of both sizes given in Eqs. (6) and (7).

$$N_{A1} = N_{A1,1} + N_{A1,2} = N_{V1}R \int_0^{R/2} f(r)dr + 2N_{V2} \int_0^{R/2} f(r)dr \quad (9)$$

Only spheres of size R contribute to the relative frequency of the circular profiles in bin $(R/2, R)$, N_{A2} . Therefore

$$N_{A2} = N_{A2,2} = 2N_{V2}R \int_{R/2}^R f(r)dr \quad (10)$$

Rewriting the above two equations in matrix form, we have

$$\begin{bmatrix} R \int_0^{R/2} f(r)dr & 2R \int_0^{R/2} f(r)dr \\ 0 & 2R \int_{R/2}^R f(r)dr \end{bmatrix} \begin{bmatrix} N_{V1} \\ N_{V2} \end{bmatrix} = \begin{bmatrix} N_{A1} \\ N_{A2} \end{bmatrix} \quad (11)$$

Since the analytical form of $f(r)$ is given in Eq. (2), the elements of the coefficient matrix can be calculated analytically. Therefore, the size distribution of spheres can be obtained by solving the above linear equations.

2.4 Random Sections of a Volume with Spheres of Radii Ranging from 0 to R

Consider a volume with randomly distributed spheres with radius range $(0, R)$. Suppose the size of spheres and their circular profiles are divided into n bins of equal width R/n . $N_A(\alpha)$ is the relative frequency of circular profiles within the α th size bin $\left((\alpha - 1)\frac{R}{n}, \alpha\frac{R}{n}\right)$, $\alpha = \overline{1, n}$. $N_V(i)$ is the relative frequency of spheres within the i th size bin $\left((i - 1)\frac{R}{n}, i\frac{R}{n}\right)$, $i = \overline{1, n}$. Using the same derivation in Step (3) (Section 2.3) Eq. (11) can be expressed as

$$\mathbf{P}\mathbf{N}_V = \mathbf{N}_A \quad (12)$$

where $\mathbf{N}_A = \{N_A(\alpha), \alpha = \overline{1, n}\}$ is a vector containing the relative frequencies of circular profiles within each size bin, $\mathbf{N}_V = \{N_V(i), i = \overline{1, n}\}$ is a vector containing the relative

frequencies of spheres within each size bin, and \mathbf{P} is an upper triangle matrix and its elements are given by

$$P(i, \alpha) = 2 \frac{iR}{n} \int_{\frac{(\alpha-1)R}{n}}^{\frac{\alpha R}{n}} f(r)dr = \frac{2R}{n} \left(\sqrt{i^2 - (\alpha - 1)^2} - \sqrt{i^2 - \alpha^2} \right), \quad (i = \overline{1, n}, \alpha = \overline{1, i}) \quad (13)$$

where $P(i, \alpha)$ denotes the portion of circular profiles in size bin α resulting from spheres in size bin i . The size distribution of spheres \mathbf{N}_V can be obtained by solving Eq. (12).

It can be seen from the above derivation that the final size distribution of circular profiles in planar sections consists of contributions from spheres in all size bins. But the radii of circular profiles associated with a sphere of a given size are all less than or equal to the sphere radius, which explains why matrix \mathbf{P} is an upper triangle matrix. Moreover, only spheres in the largest size bin contribute to the radii of circles in the largest size bin, which explains why there is only a single element in the last row in matrix \mathbf{P} . As a result, the number of spheres in the largest bin can be directly calculated. Once the number of spheres in the largest size bin is calculated, its contribution can be subtracted and the spheres in the second largest size bin become the largest spheres in the remaining distribution, which can be calculated similarly. By repeating this process, the full size distribution of spheres can be obtained from the largest to the smallest. This solution process is similar to peeling onion skins layer by layer, which explains why this approach is called the stereological unfolding process.

3 THE STEREOLOGICAL EQUATION FOR A GENERAL SPHEROID

The equation for a general spheroid is similar to the sphere equation (Eq. (12)). The primary difference is that spheres have circular profiles on planar sections, whereas spheroids have elliptical profiles. The sphere equation is essentially a one-dimensional problem that considers only the size (i.e., radius) distribution whereas the spheroid equation is a two-dimensional problem that considers both size and shape distributions (i.e., major and minor axes of ellipses). A detailed derivation can be found in Refs [18-19].

Let the size parameters U and S be the major caliper parameter of a spheroid and its planar section profile, respectively. Let V be the shape parameter of a typical spheroid and T be the random shape parameter of a random section profile. Let $F_V(u, v)$ and $F_A(s, t)$ denote the bivariate size-shape distribution functions of the spheroids and their elliptical section profiles, respectively, where $F_V(u, v) = P(U \leq u, V \leq v)$ and $F_A(s, t) = P(S \leq s, T \leq t)$. The probability of both $S > s$ and $T > t$ is given by:

$$P(S > s, T > t) = 1 - F_A(\infty, t) - F_A(s, 1) + F_A(s, t) \quad (14)$$

The stereological equation describes the relationship among the distribution functions of the spheroids and elliptical

section profiles of prolate or oblate spheroids whose principal major and minor semi-axes are a and b , respectively:

$$N_A[1 - F_A(\infty, t) - F_A(s, 1) + F_A(s, t)] = N_V \int_s^\infty \int_t^1 p(u, v, s, t) dF_V(u, v) \quad (15)$$

where $0 < s$ and $0 < t \leq 1$. The shape parameter is defined as $v = 1 - (b/a)^2$. The bi-dimensional size-shape variables (u, v) for prolate and oblate spheroids are (b, v) and (a, v) , respectively. Similarly, the size-shape parameter (s, t) for elliptical profiles is defined as $(a, 1 - (b/a)^2)$, where a and b are the principal major and minor semi-axes of the elliptical profiles, respectively [18].

4 NUMERICAL SOLUTION OF THE STEREOLOGICAL EQUATION

In real applications, the above stereological equations are usually solved numerically by discretizing the size and shape domain into “bins” or “cells”. The size and shape distributions are represented as relative frequencies or histograms over these cells. There is a close correspondence between Eq. (15) which specifies linear relations among distribution functions and linear equations which specify analogous relations among vectors of relative frequencies [18-19]. The stereological integral equation (Eq. (15)) can be transformed into a linear equation system as follows:

$$\mathbf{N}_A = \mathbf{P}\mathbf{N}_V\mathbf{Q} \quad (16)$$

where \mathbf{N}_V and \mathbf{N}_A are vectors of relative frequencies of the spheroids and their elliptical profiles, respectively. \mathbf{P} and \mathbf{Q} are transformation matrices corresponding to the kernel function $p(u, v, s, t)$ in Eq. (15). Suppose the range $(0, b)$ of size component b (or a) is divided into s bins of equal width B/s , and the range $(0, 1)$ of the shape component is divided into k bins of equal width $1/k$. The rectangular domain of variable (b, v) or (a, v) is divided into a grid comprising $s \times k$ “cells”. The relative frequency of spheroids is

$$\mathbf{N}_V = \{N_V(i, j); i = \overline{1, s}, j = \overline{1, k}\} \quad (17)$$

where $N_V(i, j)$ is the relative frequency of spheroid in cell (i, j) . Clearly, $\sum_{i=1}^s \sum_{j=1}^k N_V(i, j) = N_V$. The relative frequency of elliptical profiles is:

$$\mathbf{N}_A = \{N_A(\alpha, \beta); \alpha = \overline{1, s}, \beta = \overline{1, k}\} \quad (18)$$

where $N_A(\alpha, \beta)$ is the relative frequency of elliptical profiles in cell (α, β) . Clearly, $\sum_{\alpha=1}^s \sum_{\beta=1}^k N_A(\alpha, \beta) = N_A$. Solving Equation (16) yields

$$N_V(i, j) = \Delta^{-1} \sum_{\alpha=i}^s \sum_{\beta=j}^k p^{i\alpha} N_A(\alpha, \beta) q^{\beta j}, (i = \overline{1, s}, j = \overline{1, k}) \quad (19)$$

where $p^{i\alpha}$ and $q^{\beta j}$ are the elements of matrices \mathbf{P}^{-1} and \mathbf{Q}^{-1} , respectively. \mathbf{P} is an upper triangular matrix that is size dependent, whereas \mathbf{Q} is a lower triangular matrix that is shape dependent. The elements of matrices \mathbf{P} and \mathbf{Q} are given as follows:

$$P_{\alpha i} = \begin{cases} \sqrt{(i-1/2)^2 - (\alpha-1)^2} - \sqrt{(i-n-1/2)^2 - \alpha^2}; \\ \text{for } (\alpha = \overline{1, i-1}, i = \overline{2, s}), \\ \sqrt{i-3/4}; \text{ for } (\alpha = i, i = \overline{1, s}), \\ 0; \text{ for } (\alpha > i, i = \overline{1, s}). \end{cases} \quad (20)$$

For populations consisting of prolate spheroids, we have,

$$q_{j\beta} = \begin{cases} \sqrt{t_1^2 - 1}[f(t_\beta) - f(t_{\beta+1})]; (\beta = \overline{1, j-1}, j = \overline{2, k}) \\ \sqrt{t_1^2 - 1} f(t_j) & ; (\beta = j, j = \overline{1, k}) \\ 0 & ; (\beta > j, j = \overline{1, k}) \end{cases} \quad (21)$$

where $f(t) = t/(t^2 - 1) + \arg \tanh(t)$ and $t_\beta = [(2k - 2\beta + 2)/(2j - 2\beta + 1)]^{1/2}$.

For oblate spheroids,

$$q_{j\beta} = \begin{cases} \sqrt{1 + t_1^{-2}}[f(t_\beta) - f(t_{\beta+1})]; (\beta = \overline{1, j-1}, j = \overline{2, k}) \\ \sqrt{1 + t_1^{-2}} f(t_j) & ; (\beta = j, j = \overline{1, k}) \\ 0 & ; (\beta > j, j = \overline{1, k}) \end{cases} \quad (22)$$

where $f(t) = t/(t^2 + 1) + \arctan(t)$, $t_\beta = [(2j - 2\beta + 1)/(2k - 2j + 1)]^{1/2}$.

5 APPLICATION EXAMPLE

A FORTRAN program based on the Cruz-Orive unfolding algorithm was implemented and illustrated for a cubic section of a fictitious material containing oblate spheroidal anomalies. The spheroid samples with random values of a and b/a were generated using Monte Carlo simulation and placed at random 3D locations. The relative frequency of the samples is 1.0×10^{-4} per unit volume. The spheroid dimensions (major axis a and aspect ratio b/a) and orientation angles were modeled as independent uniformly distributed random variables with the values indicated in Table 1.

Table 1. Spheroid parameters associated with application example

Variable	Description	Lower Bound	Median	Upper Bound	Distribution
a	major axis	0.0	5.0	10.0	Uniform
b/a	aspect ratio	0.0	0.5	1.0	Uniform
$\alpha_1, \alpha_2, \alpha_3$	orientation angles	0.0	π	2π	Uniform

Table 2. Statistics of the number of ellipses on section planes

# of Sections	Average	Stdev	Min	Max
1	923	0.0	923	923
10	894.7	38.5	825	941
98	898.3	28.8	825	956

To simulate the measurements that would be obtained by the sectioning process, virtual horizontal slices were made at uniformly spaced heights within the cube. Each spheroid sample is tested against every section plane to determine whether it intersects with the section plane. If so, the major and minor axis lengths of the intercept ellipses were calculated using the ellipsoid intersection algorithm in Ref [22]. Three example cases were simulated with 1, 10, and 98 sections, respectively. Table 2 indicates the statistics of the number of ellipses per section plane for the three example cases.

The discrete size and shape distributions for both the spheroids and their elliptical profiles were obtained by dividing the size and shape parameter ranges into an equal number of bins of dimension $s \times k$. Two discretization schemes were considered: 5×5 and 10×10 . The relative frequencies of elliptical profiles per unit area N_A were used as the input for the Cruz-Orive unfolding algorithm to predict the size and shape distribution of the spheroids. The relative frequencies of the actual spheroid samples N_V^0 were used as the reference result to determine the accuracy of predictions.

Figure 5 shows the 3D histogram plots of the relative frequencies of the actual population of spheroids and the predicted population based on measurements of their elliptical profiles for the example case with 98 simulated sections. A comparison of the original distribution (Fig. 5(a)) to the predicted distribution (Fig. 5(b)) indicates reasonably similar results. Computational accuracy improves as the number of simulated sections is increased, as expected. The influence of the number of sections on predicted spheroid size parameter and shape parameter values is shown in Figs. 6 and 7, respectively for both 10×10 and 5×5 grids. For both parameters, predictions were significantly improved when the number of sections was increased from 1 to 10, but increasing the number of sections by another order of magnitude (i.e., from 10 to 100) had only a marginal improvement on prediction accuracy. This suggests that there may be an optimum number of sections that provides a good balance between computational accuracy and the number of sections (and associated costs).

Another observation from Fig. 6 is that the results are more accurate for large spheroids and the error is larger for smaller spheroids in spite of the number of sections and bins. This is an intrinsic characteristic of the unfolding algorithm because the small elliptical profiles have contributions from all spheroids with equal or larger major axes. Elliptical profiles in the largest size bin include only contribution from the spheroids in the largest size bin. The unfolding algorithm operates on the largest size bin first so errors in the large size bin propagate into the

smaller size bins, causing additional errors in smaller size bins. However, the probabilistic risk of fracture is more sensitive to large anomalies so the additional errors in the smaller anomaly sizes may have negligible influence on risk.

The primary errors associated with the stereological unfolding algorithm can be classified as statistical error (i.e., not enough Monte Carlo samples) and discretization (i.e., bin size) error. The total number of bins has an influence on both types of error. Discretization error decreases with increasing number of bins, whereas statistical error increases with increasing number of bins. The optimal number of bins is based on an optimal discretization parameter that minimizes the total error [23-24]. In practical experiments, the number of sections is limited and data noise often dominates, so the discretization error is generally insignificant compared with statistical error. For example, the accuracy of the results using 5×5 bins is

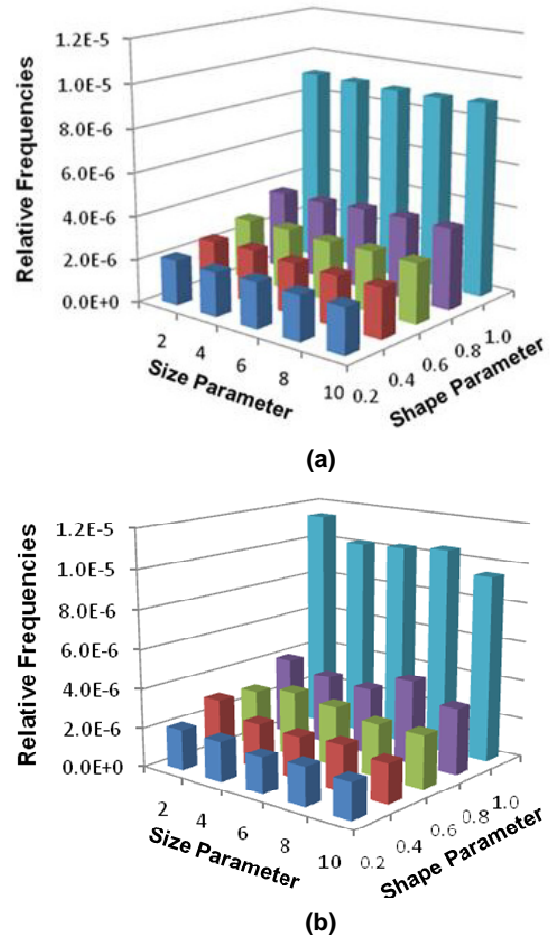
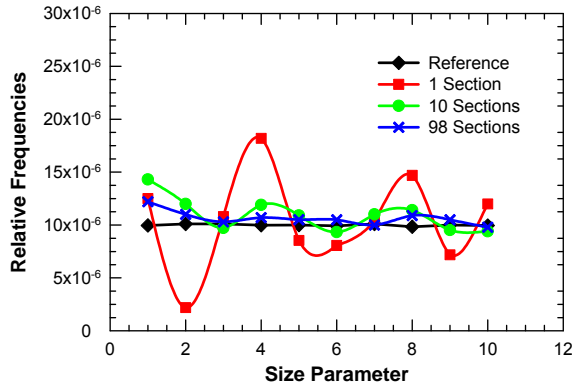
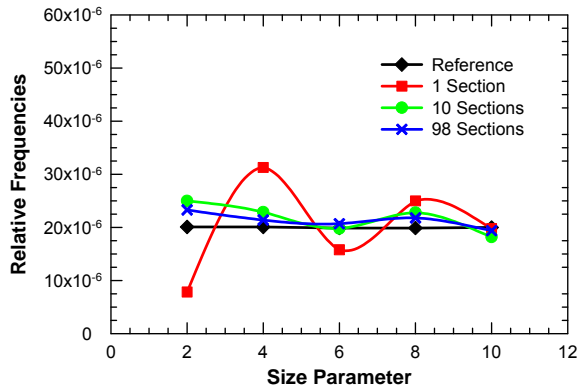


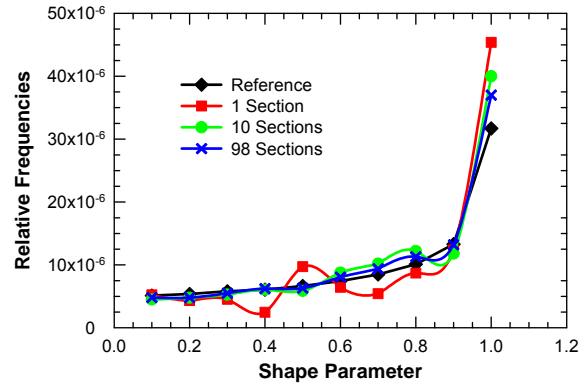
Figure 5. Bivariate histograms (stereograms) of anomaly size and shape parameters associated with anomalies in the fictitious material: (a) original population of spheroids, and (b) predicted population of spheroids based on sectioning data transformed using the Cruz-Orive unfolding algorithm.



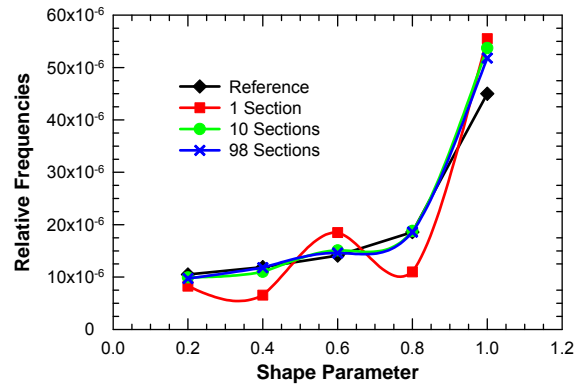
(a)



(b)



(a)



(b)

Figure 6. Influence of the number of section plane measurements on predicted spheroid size parameter values: (a) 10×10 bin grid, and (b) 5×5 bin grid.

comparable to the 10×10 bin results, if not better. Therefore, the focus should be on reducing statistical error in practical applications. It is important to have a sufficient number of samples in each bin to have small statistical errors. Ghosn [25] reported previously that the unfolding algorithm performed well for some mesh sizes and not so well for others. This difference may possibly have been due to the number of sections or the discretization bin width. Statistical error is smaller if measurements are done on more planar sections, or if the material has a higher density of spheroid centers and the spheroids are larger. However, there is a maximum limit on the density of spheroids for the Cruz-Orive stereological unfolding algorithm because this algorithm assumes that the spatial distribution of spheroids is uniform and dilute. In practice, “dilution” is satisfactory whenever the volume fraction of the spheroids to the total volume is less than about 10% [10]. This condition is required if it is assumed that the set of spheroid centers approximately forms a “Poisson ensemble” in three dimensions.

Figure 7. Influence of the number of section plane measurements on predicted spheroid shape parameter values: (a) 10×10 bin grid, and (b) 5×5 bin grid.

6 CONCLUDING REMARKS

As mentioned previously, it currently is impossible to accurately predict the shape and orientation parameters of a general ellipsoid based on measurements obtained from 2D sectioning data. If data are available in another form, such as HLS, then it may be possible to predict general ellipsoid parameters by combining the data using Bayesian updating or a similar method. On the other hand, if data are only available from 2D sectioning, then a general ellipsoid model is probably not an appropriate one because it simply cannot be fully characterized. In this situation, the anomaly model should be limited to either the prolate or oblate spheroid model.

In this study, an unfolding algorithm was implemented and verified that can be used to estimate the dimensions and orientations of 3D spheroids based on 2D sectioning measurements. It was shown that the accuracy of the predicted spheroid model is dependent on the number of sections and the discretization of the mesh used to characterize the data. In some instances, the number of sections may be a fixed quantity (e.g., historical data). In this case, the unfolding algorithm

could be used to quantify confidence bounds on fracture risk associated with the uncertainty in the spheroid model for the fixed number of sections. For new design, the number of sections is probably limited by the cost to obtain them. In this situation, the unfolding algorithm could be used to identify the minimum number of sections that would be required to meet a fracture risk reliability target that accounts for the uncertainty associated with the number of sections.

In this study it was assumed that anomalies could have any orientation, and that all orientations were equally likely to occur. It was further assumed that each anomaly would be intersected by a single plane. Under these constraints, it is impossible to determine the out-of-plane dimensions of a sectioned anomaly which are needed to characterize a 3D ellipsoidal model. However, in some materials the anomaly orientation may be influenced by processing conditions that may result in an overall bias in orientation. For example, previous studies (e.g., [25] among others) suggest that the longest dimension of the anomaly may be aligned with the direction of forging strains, which could provide additional information for use in characterizing an ellipsoidal model. Although this relationship is not well understood and has not been validated, it could lead to the development of improved anomaly models in the future.

ACKNOWLEDGMENT

This work was supported by the NASA Glenn Research Center under Contract NNC08CB06C.

REFERENCES

- [1] National Transportation Safety Board, 1990, "Aircraft Accident Report - United Airlines Flight 232 McDonnell Douglas DC-10-10 Sioux Gateway Airport, Sioux City, Iowa, July 19, 1989," *NTSB/AAR-90/06*, National Transportation Safety Board, Washington, DC.
- [2] National Transportation Safety Board, 1996, "Aircraft Accident Report – Uncontained Engine Failure, Delta Air Lines Flight 1288, McDonnell Douglas MD-88, N927DA," *NTSB/AAR-98/01*, National Transportation Safety Board, Washington, DC.
- [3] Roth, P.G., 1992, "Probabilistic Rotor Design System (PRDS) Phase I," *WL-TR-92-2011*, GE Aircraft Engines.
- [4] Adamson, J.D., Fox, E.P., and Malone, J.E., 1995, "Probabilistic Design System – Phase I and II Interim Report," *Pratt & Whitney Report, FR-24004-1*.
- [5] Leverant, G.R., Littlefield, D.L., McClung, R.C., Millwater, H.R., and Wu, Y-T., 1997, "A Probabilistic Approach to Aircraft Turbine Material Design," *Proceedings of the 42nd ASME International Gas Turbine & Aeroengine Technical Congress*, Paper 97-GT-22.
- [6] Millwater, H., Fitch, S., Wu, Y-T., Riha, D., Enright, M., Leverant, G., McClung, C., Kuhlman, C., Chell, G., and Lee, Y., 2000, "A Probabilistically-Based Damage Tolerance Analysis Computer Program for Hard Alpha Anomalies in Titanium Rotors," *Proceedings of the 45th ASME International Gas Turbine & Aeroengine Technical Congress*, Munich, Germany, Paper No. 2000-GT-0421.
- [7] Leverant, G.R., McClung, R.C., Millwater, H.R., and Enright, M.P., 2003, "A New Tool for Design and Certification of Aircraft Turbine Rotors," *Journal of Engineering for Gas Turbines and Power*, ASME, Vol. 126, No. 1, pp. 155-159.
- [8] McClung, R.C., Enright, M.P., Millwater, H.R., Leverant, G.R., and Hudak, S.J., 2004, "A Software Framework for Probabilistic Fatigue Life Assessment," *Journal of ASTM International*, 1 (8) Paper ID JAI11563. Also published in *Probabilistic Aspects of Life Prediction*, *ASTM STP 1450*, pp. 199-215.
- [9] Southwest Research Institute, 2010, *DARWIN® User's Guide*. Southwest Research Institute, San Antonio, TX.
- [10] Federal Aviation Administration, 2001, "Advisory Circular – Damage Tolerance for High Energy Turbine Engine Rotors," *AC 33.14-1*, U.S. Department of Transportation, Washington, DC.
- [11] Federal Aviation Administration, 2009, "Advisory Circular – Guidance Material for Aircraft Engine Life-Limited Parts Requirements," *AC 33.70-1*, U.S. Department of Transportation, Washington, DC.
- [12] Federal Aviation Administration, 2009, "Advisory Circular – Damage Tolerance of Hole Features In High-Energy Turbine Engine Rotors," *AC 33.70-2*, U.S. Department of Transportation, Washington, DC.
- [13] Wu, Y.-T., Enright, M.P., McClung, R.C., Millwater, and H., Leverant, G.R., 2000, "Probabilistic Methods for Design Assessment of Reliability With Inspection," *Proceedings, 41st Structures, Structural Dynamics, and Materials Conference*, Atlanta, GA, April 3-6.
- [14] Enright, M.P. and Wu, Y.-T., 2000, "Probabilistic Fatigue Life Sensitivity Analysis of Titanium Rotors," *Proceedings of the 41st Structures, Structural Dynamics, and Materials Conference*, Atlanta, GA, April 3-6, AIAA Paper 2000-1647.
- [15] Wicksell, S.D., 1925, "The Corpuscle Problem I: Case of Spherical Corpuscles," *Biometrika*, Vol. 17, pp. 84-99.
- [16] Wicksell, S.D., 1926, "The Corpuscle Problem II: Case of Ellipsoidal Corpuscles," *Biometrika*, Vol. 18, pp. 151-172.
- [17] Moran, P.A.P., 1972, "The Probabilistic Basis of Stereology," *Suppl. Adv. Appl. Prob.*, pp. 69.
- [18] Cruz-Orive, L.M., 1976, "Particle Size-Shape Distributions: the General Spheroid Problem I: Mathematical Model," *Journal of Microscopy*, Vol. 107, pp. 235-253.
- [19] Cruz-Orive, L.M., 1977, "Particle Size-Shape Distributions: the General Spheroid Problem II: Stochastic Model and Practical Guide," *Journal of Microscopy*, Vol. 112, pp. 153-167.

- [20] Hilliard, J.E., Lawson, L.R., 2003, *Stereology and Stochastic Geometry*, Kluwer Academic Publishers, Norwell, MA, USA, pp. 308-312.
- [21] S. Saltykov, 1967, "The Determination of the Size Distribution of Particles in an Opaque Material from a Measurement of the Size Distribution of Their Sections," in *Stereology, Proceedings of the Second International Congress for Stereology*, H. Elias, (Ed.), Springer Verlag, New York, pp. 163-167.
- [22] Pope, S.B., 2008, "Algorithms for Ellipsoids," *Cornell University Report FDA 08—01*, Cornell University.
- [23] Ohser, J. and Mücklich, F., 2000, *Statistical Analysis of Microstructures in Material Science*, John Wiley & Sons, LTD, West Sussex, England, ISBN 0-471-97486-2.
- [24] Ohser, J. and Sandau, K., 2000, "Considerations about the Estimation of the Size Distribution in Wicksell's Corpuscle Problem," in *Statistical Physics and Spatial Statistics*, Mecke and Stoyan (Eds), Springer-Verlag, New York, ISBN: 3-540-67750-X, pp. 185-202.
- [25] Ghosn, L.J., Kantzos, P.T., Barrie, R.L., and Bonacuse, P.J., 2003, "Unfolding the Ceramic Inclusion Size Distribution in a Powder Metallurgy Alloy from Planar Sections," *Materials Science and Technology 2003*, Chicago, Illinois, November 11, 2003 (presentation only).